Optical conductivity of metal alloys with residual resistivities near or above the Mott-Ioffe-Regel limit

G. D. Samolyuk,[1,*] C. C. Homes,[2] A. F. May,[1] S. Mu,[1,†] K. Jin,[1] H. Bei,[1] G. M. Stocks,[1] and B. C. Sales[1,‡]

[1]*Materials Science and Technology Division, Oak Ridge National Laboratory, Oak Ridge, Tennessee 37831, USA*

[2]*Condensed Matter Physics and Materials Science Department, Brookhaven National Laboratory, Upton, New York 11793, USA*

Most interesting examples of violations of the Mott-Ioffe-Regel (MIR) resistivity limit are found in materials with strong electronic correlations that are not well understood by theory. We demonstrate that first principles theory can predict the experimentally observed frequency dependence of the optical conductivity for a novel class of metals where the residual resistivity is near or above the MIR limit, which we define as a "bad metal." The predicted optical conductivity of a NiCoCr alloy is in good agreement with experiment. It is demonstrated that the width of the Drude peak describing the low-frequency part of optical conductivity is comparable to the Fermi energy. The latter, together with a mean free path comparable to the interatomic distance, indicates the absence of well-defined quasiparticles. In contrast to traditional bad metals with strong electron-electron interactions, both the high resistivity and the large width of the Drude peak in these alloys result from strong scattering on disordered atomic potentials that can be understood using modern density functionals.

I. INTRODUCTION

A linear electrical resistivity at low temperatures is often connected to interesting physics. In cuprate, iron-based and organic superconductors, heavy fermion materials, and some complex $4d$ oxides such as $Sr_3Ru_2O_7$, it is associated with the proximity to a quantum critical point [1,2]. In some of these systems the linear resistivity persists up to high temperatures even when the resistivity is well above the Mott-Ioffe-Regel (MIR) limit for a crystalline solid [3,4]. Crystalline metals where the resistivity exceeds the MIR limit have been termed "bad metals" [5,6]. Transport in bad metals is governed by the collective diffusion of energy and charge rather than by quasiparticle or momentum relaxation [5]. Unfortunately, transport in strongly correlated materials is not well understood theoretically due to the difficulty in incorporating the strong electron-electron interactions into even the simplest model Hamiltonians such as the Hubbard model [7].

Concentrated solid solutions (CSSs) with multiple principle elements are a relatively new class of crystalline solids, with perhaps high-entropy alloys (HEAs) as the most familiar examples (e.g., NiFeCoCrMn). In these alloys all elements are distributed randomly on a face-centered-cubic (fcc) or body-centered-cubic (bcc) lattice, with each element present in approximately the same concentration. In such alloys the configurational entropy at the formation temperature plays an essential role in their stabilization [8–11]. Several of these alloys have remarkable mechanical properties and resistance to radiation damage [10,12,13]. Large single crystals of many HEA alloys have crystalline qualities (e.g., mosaic spread, ion channeling properties) comparable to single crystals of a single element [12,14,15]. The disorder in these alloys is controlled in the sense that the alloys are homogeneous from the centimeter to the subnanometer scale and each element sits very close to an ideal lattice site for a fcc structure [16].

Previously, we experimentally and theoretically surveyed the resistivity of a large number of Ni based CSS alloys [16–18]. An initial theoretical analysis predicted that several of the alloys containing Mn or Cr were potentially "bad metals" with residual resistivities near or above the MIR limit [16,18]. However, one of these alloys, NiCoCr (sometimes referred to as a medium entropy alloy) [13] also exhibited a resistivity linear in temperature down to very low temperatures, at least 0.5 K, albeit with a large residual resistivity (Fig. 1). Further study indicated that NiCoCr is also near a quantum critical point separating a ferromagnetic and a paramagnetic metal, with critical exponents in excellent agreement with Belitz, Kirkpatrick, Vojta theory [15,19]. Although density functional theory (DFT) cannot address details of quantum criticality, it can address the large residual resistivity of NiCoCr, which dominates the resistivity and the optical conductivity. One huge advantage of investigating CSS alloys, such as NiCoCr, rather than a strongly correlated material, is that a particular implementation of DFT that is designed to directly calculate the configurationally averaged properties of disordered alloys [22–24] has been remarkably successful in understanding the electronic and transport properties of CSS alloys [12,16,18]. In the present work we examine both theoretically and experimentally whether NiCoCr is a bad metal and compare the results to NiCoFe, an alloy with well-defined quasiparticles and normal Fermi liquid behavior. We show that the predicted low-frequency optical conductivity of NiCoCr as a function of energy is in good agreement with the experimental results.

*samolyukgd@ornl.gov

†Present address: Materials Department, University of California, Santa Barbara, CA 93106, USA.
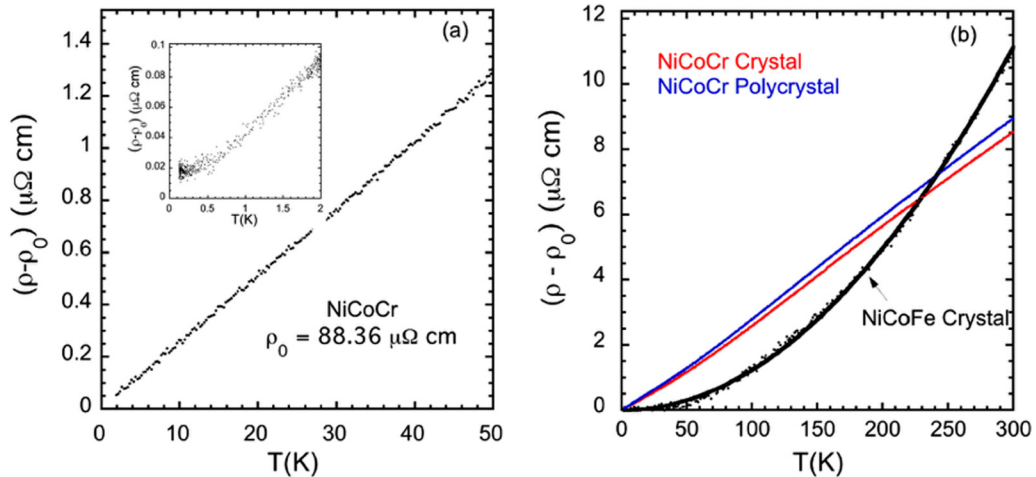
‡salesbc@ornl.gov

FIG. 1. (a) Resistivity of NiCoCr below 50 K illustrating the *T*-linear dependence. Inset shows linear behavior persists to ≈0.5 K. Note, however that the total resistivity only changes by about 10% from 0.1 to 300 K because of the large residual resistivity (see Supplemental Material [20]). The large residual resistivity is due to the chemical disorder in this alloy and can be calculated using modern density functional theory. (b) Comparison of resistivity of NiCoCr with that of NiCoFe. The residual resistivity, ρ_0, for NiCoFe is ≈5.3 $\mu\Omega$ cm as compared to ≈88 $\mu\Omega$ cm for NiCoCr. For $T < 15$ K the resistivity of NiCoFe is accurately described by $\rho_0 + AT^2$, with $A = 5.8 \times 10^{-5} (\mu\Omega \, \text{cm} \, \text{K}^{-2})$. The T^2 dependence of the resistivity of NiCoFe is consistent with the expectations of Fermi liquid theory. The coefficient A is about two times larger than the value for pure iron [21].

In contrast to traditional metals, the almost conserved momentum operator does not exist in a bad metal. It can be shown, however, that momentum decay is characterized by a momentum relaxation rate, Γ, which can be estimated from the low-frequency response of the optical conductivity $\sigma(\omega) \sim 1/(-i\omega + \Gamma)$. In NiCoCr the value of Γ is predicted to be almost 2 eV, an energy scale comparable to the width of the *d* bands, which are of the order of 3–5 eV. In a normal metal, such as Ni, the room temperature value [25] of Γ is about 0.04 eV. As was demonstrated by Allen [26] who showed the relationship between the memory function and the electron self-energy [27], the information from the low-frequency optical conductivity allows us to estimate the $\omega \to 0$ limit for the imaginary part of electron self-energy averaged over the Fermi surface. Thus, the width of the Drude approximant to the infrared optical conductivity allows us to make a conclusion about quasiparticle lifetimes and the applicability of the quasiparticle approach for the system in general.

II. METHODOLOGY

A. Crystal growth and resistivity

Single crystals of NiCoCr and NiCoFe were grown using the floating zone method as described previously [14,15]. The crystals used for the optical measurements were oriented and cut from a large boule using an electrodischarge machine. The (100) face was mechanically polished. To remove the damage created during polishing, the surface was then electropolished with an 85% H3PO4 solution using a bias of about 10 V. Small bars from the same crystal were used for standard four-probe resistivity measurements [15]. Four thin Pt wires (0.002-in.) were spot welded to each sample. The total resistivity of NiCoCr is shown in Fig. S1 in the Supplemental Material [20].

B. Optical measurements

The reflectance has been measured at room temperature at a near-normal angle of incidence, using Bruker IFS 113v and Vertex 80v spectrometers, over a wide frequency range from the terahertz (~2 meV) to the ultraviolet (5 eV) regions using an *in situ* evaporation technique [28]. The complex optical conductivity is determined from a Kramers-Kronig analysis of the reflectance, which requires extrapolations in the $\omega \to 0, \infty$ limits [29]. At low frequency, a metallic Hagen-Rubens extrapolation is employed, $R(\omega) = 1 - a\sqrt{\omega}$, where a is chosen to match the data at the lowest measured frequency point. Above the highest measured frequency the reflectance of Cr [30] has been scaled to match the data and is used up to ~35 eV, above which a free-electron gas asymptotic reflectance extrapolation $R(\omega) \propto 1/\omega^4$ is assumed [31].

C. Details of calculations

In the case of incoherent metals, the Boltzmann equation approach fails due to the absence of well-defined quasiparticles [32–34]. On the other hand, the Kubo-Greenwood (KG) approach [35,36] to the calculation of the conductivity does not suffer from this problem [37] since it deals directly with the current-current correlation function. The expression for optical conductivity at zero temperature is defined as follows [38]:

$$\sigma_{\alpha\alpha}(\omega) = \frac{1}{V\omega\pi} \int_{E_F+\hbar\omega}^{E_F} d\varepsilon \text{Tr} \langle \text{Im} G(\varepsilon) j_\alpha \text{Im} G(\varepsilon + \hbar\omega) j_\alpha \rangle,$$
(1)

where V is the volume of the system; E_F is Fermi energy; $G(\varepsilon)$ is the Green's function of the system; and $j_\alpha = -ie/\hbar [r_\alpha, \hat{H}]$ is an electric current operator calculated using the commutator of the radius vector, r_α, and Hamiltonian, $\hat{H}$ (see Ref. [39]

for the details). The brackets imply configurational average over all possible atomic distributions in the alloy. Earlier, in a series of publications (see, for example, Ref. [40,41]) it was demonstrated that the vertex correction [42] contribution to the conductivity calculation can be neglected in the case of the transition metals. After neglecting vertex corrections Eq. (1) is reduced to

$$\sigma_{\alpha\alpha}(\omega) = \frac{1}{V\omega\pi} \int_{E_F + \hbar\omega}^{E_F} d\varepsilon \, \text{Tr}\,\text{Im}\bar{G}(\varepsilon)j_\alpha \text{Im}\bar{G}(\varepsilon + \hbar\omega)j_\alpha, \quad (2)$$

where $\bar{G}$ is the configurationally averaged Green's function.

This expression allows us to calculate the optical conductivity using the coherent potential approximation (CPA) [22,23] together with a multiple scattering formalism [24]. CPA is a mean-field-type approximation which restores the translational invariance of an alloy by substitution of an effective value for the scattering matrix of each particular atom. The effective scattering t matrix is obtained self-consistently from the constraint that preserves the average scattering properties of a single impurity in the effective medium. Notably, the effective CPA t matrix corresponds to a complex scattering potential that is absorptive, directly leading to a finite residual resistivity. It has been demonstrated that CPA is the best single-site approximation for metal alloys. Calculations of the Green's function, $\bar{G}$, in Eq. (2) of the disordered alloys were performed using a version of the Korringa–Kohn–Rostoker CPA (KKR-CPA) method [43] implemented within DFT [44]. The calculations used the experimental lattice parameter for all alloys. To allow for the possibility of a ferromagnetic ground state, the exchange correlation was treated within the local spin density approximation (LSDA) to DFT using the Barth-Hedin [45] functional. It was found that the result for static conductivity calculated in the generalized gradient approximation (GGA) deviates from the LSDA results by approximately 15% [16]. A $34 \times 34 \times 34$ mesh has been used for Brillouin zone integration.

It should be mentioned that the temperature dependence of the optical conductivity could be introduced into the calculation in a manner similar to that used for calculating the dc conductivity (see [18]). In the case of NiCoCr the temperature dependence comes primarily from electron scattering on lattice vibrations. The electron lattice scattering can be incorporated into the calculation using an alloy analogy [46,47]. Using this approach the temperature dependent static conductivity has been calculated for temperatures up to 1200 K. At higher temperatures a supercell approach is required due to large atomic displacements expansion convergence problems. The temperature dependence of optical conductivity was not addressed in the current paper since the resistivity of this alloy only changes by about 10% upon heating to 300 K, the temperature of optical conductivity measurements.

Also, any type of localization cannot be addressed by a CPA approach. This effect can be captured by the typical medium approach [48,49]. However, this subject is out of the scope of the current paper.

III. RESULTS AND DISCUSSION

To be consistent with experimental results, the NiCoCr alloy was treated in our calculations as nonmagnetic [50], while the NiCoFe alloy is treated as a ferromagnetic alloy with resulting averaged magnetic moments equal 0.6, 1.6, and 2.6 μ_B for Ni, Co, and Fe, respectively. Details about the electronic structure of the alloys are discussed in our previous publications [12,16,18,51]. The spin-resolved electronic density of states (DOS) are shown in the right inset in Figs. 2(a) and 2(b), and 2(c) and 2(d) for the NiCoFe and NiCoCr alloys, respectively. In the figure, the Fermi energy is taken as zero energy. For each alloy panel, the top (bottom) panels correspond to the DOS of majority- (minority-) spin states, respectively. Within each panel, the red (green, blue) lines correspond to the Ni (Co, Fe/Cr) local DOS. Similarly, the horizontal dashed red (solid green, dotted blue) lines denote
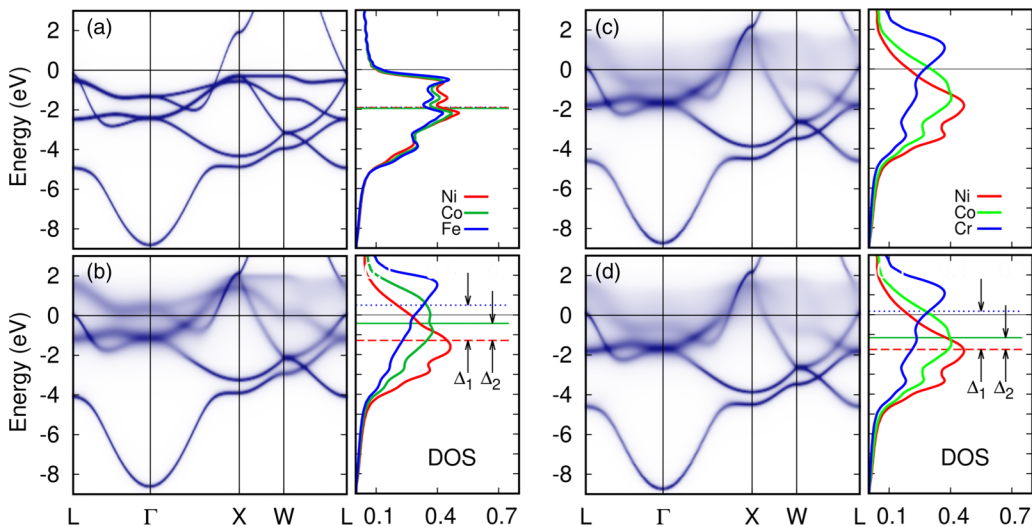

FIG. 2. Calculated CPA Bloch spectral function (BSF) and partial density of states for NiCoFe (a,b) and NiCoCr (c,d) for the majority- (a,c) and minority- (b,d) spin channels, respectively. The splitting between the d-electron band centers of Ni and Fe is denoted by Δ_1 and for Ni and Co, as Δ_2 in the NiCoFe in the minority-spin channel. For NiCoCr, Δ_1 and Δ_2 correspond to the splitting of Ni-Cr and Ni-Co d-electron resonances, respectively. Since NiCoCr is paramagnetic, there is no difference between the majority- and minority-spin channels.
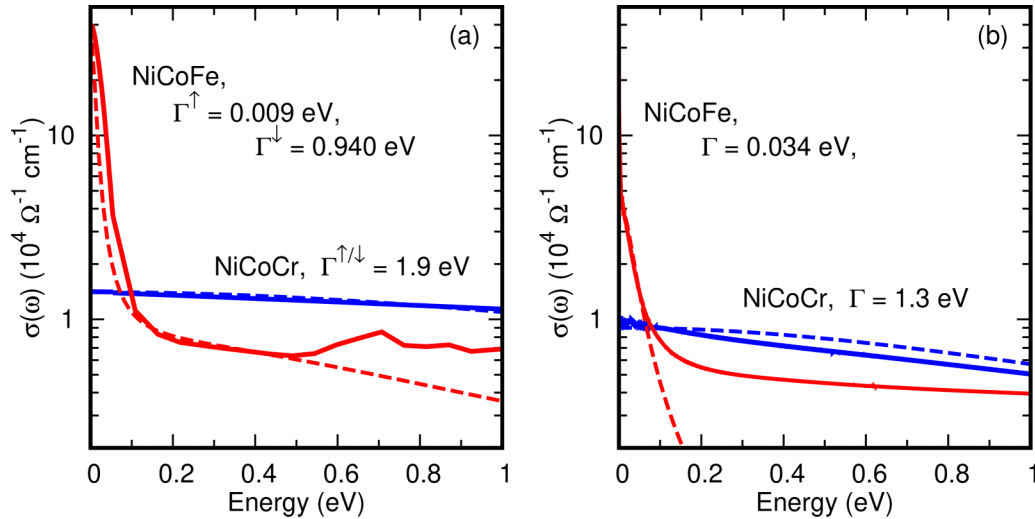
FIG. 3. Theoretical prediction of optical conductivity for NiCoCr (solid blue) and NiCoFe (solid red). Both NiCoCr and NiCoFe are single-crystal alloys with electropolished surfaces. A Drude fit to the theoretical conductivity was calculated for each spin channel separately and the sum is shown by the dashed red line. Since NiCoCr is nonmagnetic there is no difference between the two spin channels. (b) Experimental optical conductivity. The dashed red and blue lines are Drude fits to the experimental data. Also see Fig. S2 in the Supplemental Material [20].

the centers of gravity of the Ni (Co, Fe/Cr) spin-resolved d bands. A Cr atom contains five d electrons and has half-filled d bands whereas Fe, Co, and Ni have almost-filled d bands. As a result, the electronic structure from these two groups behaves differently upon alloying [12,16,18]. The occupation of d bands and the resulting position of the Fermi level can be approximately obtained by minimization of the band structure energy, E_b, together with additional constraints to preserve atomic charge neutrality. In alloys comprising elements with similar numbers of d electrons (Fe, Co, Ni) E_b minimization results in the alignment of majority-spin d states. In NiCoFe this leads to almost negligible splitting, Δ_1, Δ_2 between Ni-Fe and Ni-Co d band centers. This corresponds to weak scattering in the majority-spin channel, and a high dc conductivity, $\sigma(0)$, in this channel. The splitting in the minority-spin channel can be estimated from the relation between exchange splitting and the size of the magnetic moment of each element [51]. The splitting [52] is $\Delta E_d = E_d^\uparrow - E_d^\downarrow = I \cdot m$, where the Stoner parameter $I \sim 1 \, \text{eV}/\mu_B$ in $3d$ transition metals and m is the magnetic moment of each element in units of μ_B. Since the d-band centers of the majority-spin states, $E_d^\uparrow$, are the same for each component, $\Delta_1 \sim 2 \, \text{eV}$ and $\Delta_2 \sim 1 \, \text{eV}$ (see Fig. 2). The large difference in the number of d electrons between Cr and Ni or Co does not allow alignment of the d bands of each component while preserving atomic charge neutrality. Together with an absence of spin polarization, this results in a large d-band splitting, $\Delta_1 \sim 2 \, \text{eV}$ and $\Delta_2 \sim 0.8 \, \text{eV}$, in both spin channels with significant electron scattering and, as a result, a small $\sigma(0)$ value.

The strong scattering in d channels results in significant broadening of the d-"band" Bloch spectral function (BSF) (see Fig. 2), this being the generalization of the band structure of an ordered system to include disorder. Thus, the majority-spin BSF in NiCoFe [Fig. 2(a)], is characterized by well-defined bands similar to pure Ni. In the minority-spin channel in NiCoFe, and for both spin channels in NiCoCr, a large splitting of the d band results in strong d-electron scattering which

is seen as a large broadening (on the scale of dimension of the Brillouin zone) of the BSF within the d-band region—and the Fermi energy in particular. In NiCoFe one consequence of the large disparity between transport in the majority- versus minority-spin channels is that an electrical current in NiCoFe is highly spin polarized, a feature of interest for possible spintronic applications. By contrast electrons in the NiCoCr alloy cannot be described as a Fermi liquid, i.e., a system with long-lived weakly interacting quasiparticles. This statement is also confirmed by the properties of the low-frequency optical conductivity.

The calculated optical conductivities for NiCoCr and NiCoFe illustrate dramatically different low-frequency behaviors [Fig. 3(a)]. To analyze this disparate behavior, the calculated $\sigma(\omega)$ was fit to the Drude model,

$$\sigma(\omega) = \frac{\sigma(0)}{1 + (\hbar\omega/\Gamma)^2}, \quad (3)$$

where Γ is the momentum relaxation rate. For NiCoFe the optical conductivities for the majority- and minority-spin channels, along with the fitted values of Γ, were calculated separately. For NiCoFe Γ equals 0.009 and 0.94 eV for the majority- and minority-spin channels, respectively. Since NiCoCr is a paramagnet there is no difference between the majority- and minority-spin channels and the predicted value of Γ is 1.9 eV. The Γ values for both alloys are also shown in Fig. 3(a). The measured optical conductivities for NiCoCr and NiCoFe at 300 K are shown in Fig. 3(b) and the agreement with the theoretical prediction is remarkable. The experimental values for Γ are 0.03 eV for NiCoFe and 1.3 eV for NiCoCr. The somewhat larger experimental value of Γ for NiCoFe as compared to the prediction by theory is due in part to the temperature of the measurement since the calculations assume $T = 0$, and to the effect of the minority-spin conductivity which is ignored in fitting the experimental data. Also the resistivity of the NiCoFe alloy changes by a factor of 3 (5.3–16.3 $\mu\Omega$ cm) from $T = 0$ to 300 K, which nicely

accounts for the difference between the experimental and theoretical results at very low frequencies. However, both theory and experiment find very large Γ values ≈ 1–$2\,\mathrm{eV} \approx E_F$ for NiCoCr.

In addition, theoretical calculations predict that the zero temperature electron mean free path in NiCoCr equals 4 Å [18], which is very close to the lattice parameter, 3.559 Å; i.e., there are no well-defined quasiparticles. This result also suggests that for NiCoCr the resistivity is already close to the MIR limit at $T = 0$.

IV. CONCLUSIONS

The combination of first principles theory and experiment clearly demonstrate that NiCoCr is a bad metal. Although the theory is a mean-field implementation of density functional theory, it captures many of the features of NiCoCr and similar alloys. It correctly predicts the optical conductivity and the residual resistivity [16] of these alloys to within about 25%. Not surprisingly, other features of NiCoCr are not captured by a mean-field theory, such as the linear resistivity ($\rho - \rho_0$) at very low temperatures and scaling details of the magnetic response. These features are associated with the proximity of NiCoCr to a quantum critical point [15]. However, the total resistivity of NiCoCr at all temperatures is dominated by the residual resistivity, which can be treated by first principles. It is worth noting that the shape of the Drude peak for NiCoCr only weakly depends on whether the ground state is assumed to be magnetically ordered (see Supplemental Material, Fig. S4 [20]).

While bad metals are normally associated with strong electron-electron correlations, the foregoing results and analysis strongly suggest that the controlled disorder present in NiCoCr and related high-entropy alloys containing Mn or Cr appears to represent another path to a bad metal. Furthermore, it is one that can be predicted within the context of modern DFT electronic structure theory. In these highly crystalline alloys strong electron scattering on disordered atomic potentials is the source of the large residual resistivity. Another beautiful example of the effects of controlled disorder was recently reported for a graphene bilayer where one layer was twisted by a small angle ($\approx 0.1°$) with respect to the other layer. The system behaved almost identically to a Mott insulator like La_2CuO_4, including the response to doping [54] despite the absence of strong electron correlations. The graphene results and the results reported here suggest that certain types of controlled disorder are more tractable by theory and may be an interesting route to produce behavior normally only seen in strongly correlated materials.

[1] L. Taillefer, Superconductivity and quantum criticality, Phys. Canada **67**, 109 (2011).

[2] J. A. N. Bruin, H. Sakai, R. S. Perry, and A. P. Mackenzie, Similarity of scattering rates in metals showing T-linear resistivity, Science **339**, 804 (2013).

[3] M. Gurvitch, Ioffe-Regel criterion and resistivity of metals, Phys. Rev. B **24**, 7404 (1981).

[4] O. Gunnarsson, M. Calandra, and J. E. Han, Colloquium: Saturation of electrical resistivity, Rev. Mod. Phys **75**, 1085 (2003).

[5] S. A. Hartnoll, Theory of universal incoherent metallic transport, Nat. Phys. **11**, 54 (2015).

[6] V. J. Emery and S. A. Kivelson, Superconductivity in Bad Metals, Phys. Rev. Lett. **74**, 3253 (1995).

[7] H. Tasaki, The Hubbard model—an introduction and selected rigorous results, J. Phys.: Condens. Matter **10**, 4353 (1998).

[8] B. Cantor, I. T. H. Chang, P. Knight, and A. J. B. Vincent, Microstructural development in equiatomic multicomponent alloys, Mater. Sci. Eng. A **375–377**, 213 (2004).

[9] Z. Wu, H. Bei, G. M. Pharr, and E. P. George, Recovery, recrystallization, grain growth, and phase stability of a family of FCC-structured multicomponent equiatomic solid solution alloys, Intermetallics **46**, 131 (2014).

[10] B. Gludovatz, A. Hohenwarter, D. Catoor, E. H. Chang, E. P. George, and R. O. Ritchie, A fracture-resistant high-entropy alloy for cryogenic applications, Science **345**, 1153 (2014).

[11] C. M. Troparevsky, J. R. Morris, P. R. C. Kent, A. R. Lupini, and G. M. Stocks, Criteria for Predicting the Formation of Single-Phase High-Entropy alloys, Phys. Rev. X **5**, 011041 (2015).

[12] Y. Zhang *et al.*, Influence of chemical disorder on energy dissipation and defect evolution in nickel and nickel-based concentrated solid solution alloys, Nat. Commun. **6**, 8736 (2015).

[13] B. Gludovatz, A. Hohenwarter, K. V. S. Thurston, H. Bei, Z. Wu, E. P. George, and R. O. Ritchie, Exceptional damage-tolerance of a medium entropy alloy CrCoNi at cryogenic temperatures. Nat. Commun. **7**, 10602 (2016).

[14] Z. Wu, Y. F. Gao, and H. Bei, Single crystal plastic behavior of a single phase, face centered cubic, equiatomic FeNiCrCo alloy, Scr. Mater. **109**, 108 (2015).

[15] B. C. Sales, K. Jin, H. Bei, J. Nichols, M. F. Chisholm, A. F. May, N. P. Butch, A. D. Christianson, and M. A. McGuire, Quantum critical behavior in the asymptotic limit of high disorder in the medium entropy alloy $NiCoCr_{0.8}$, npj Quantum Mater. **2**, 33 (2017).

[16] S. Mu, G. D. Samolyuk, S. Wimmer, M. C. Troparevsky, S. N. Khan, S. Mankovsky, H. Ebert, and G. M. Stocks, Uncovering electron scattering mechanisms in NiFeCoCrMn derived concentrated solid solution and high entropy alloys, npj Comput. Mater. **5**, 1 (2019).

[17] K. Jin, B. C. Sales, G. M. Stocks, G. D. Samolyuk, M. Daene, W. J. Weber, Y. Zhang, and H. Bei, Tailoring the physical properties of Ni-based single phase equiatomic alloys by modifying the chemical complexity, Sci. Rep. **6**, 20159 (2016).

[18] G. D. Samolyuk, S. Mu, A. F. May, B. C. Sales, S. Wimmer, S. Mankovsky, H. Ebert, and G. M. Stocks, Temperature dependent electronic transport in concentrated solid solutions of the $3d$-transition metals Ni, Fe, Co and Cr from first principles, Phys. Rev. B **98**, 165141 (2018).

[19] T. R. Kirkpatrick and D. Belitz, Exponent relations at quantum phase transitions with applications to metallic quantum ferromagnets, Phys. Rev. B **91**, 214407 (2015).

[20] See Supplemental Material at http://link.aps.org/supplemental/10.1103/PhysRevB.100.075128 for total resistivity temperature dependence (Fig. S1) and for experimental optical conductivity for NiCoCr and NiCoFe (Fig. S2) contains Ref. [53].

[21] M. Isshiki and K. Igaki, Temperature dependence of the electrical resistivity of pure iron at low temperatures, Trans. Jpn. Inst. Met. **19**, 431 (1978).

[22] P. Soven, Coherent-potential model of substitutional disordered alloys, Phys. Rev. **156**, 809 (1967).

[23] W. D. Taylor, Vibrational properties of imperfect crystals with large defect concentrations, Phys. Rev. **156**, 1017 (1967).

[24] G. M. Stocks, W. M. Temmerman, and B. L. Gyorffy, Complete Solution of the Korringa-Kohn-Rostoker Coherent-Potential-Approximation Equations: Cu-Ni Alloys, Phys. Rev. Lett. **41**, 339 (1978).

[25] M. A. Ordal, R. J. Bell, R. W. Alexander, L. L. Long, and M. R. Querry, Optical properties of fourteen metals in the infrared and far infrared: Al, Co, Cu, Au,Fe, Pb, Mo, Ni, Pd, Pt, Ag, Ti, V, and W, Appl. Opt. **24**, 4493 (1985).

[26] P. B. Allen, Electron self-energy and generalized Drude formula for infrared conductivity of metals, Phys. Rev. B **92**, 054305 (2015).

[27] W. Götze and P. Wölfle, Homogeneous dynamical conductivity of metals, Phys. Rev. B **6**, 1226 (1972).

[28] C. C. Homes, M. Reedyk, D. A. Crandles, and T. Timusk, Technique for measuring the reflectance of irregular, submillimeter-sized samples, Appl. Opt. **32**, 2976 (1993).

[29] M. Dressel and G. Grüner, *Electrodynamics of Solids* (Cambridge University Press, Cambridge, 2001).

[30] D. W. Lynch, W. R. Hunter, and E. D. Palik (Academic, New York, 1991), p. 374.

[31] F. Wooten, *Optical Properties of Solids* (Academic, New York, 1972), pp. 244–250.

[32] J. M. Ziman, *Electrons and Phonons: The Theory of Transport Phenomena in Solids* (Oxford University Press, Oxford, 1960).

[33] P. B. Allen, New method for solving Boltzmann's equation for electrons in metals, Phys. Rev. B **17**, 3725 (1978).

[34] S. Y. Savrasov and D. Y. Savrasov, Electron-phonon interactions and related physical properties of metals from linear-response theory, Phys. Rev. B **54**, 16487 (1996).

[35] R. Kubo, Statistical-mechanical theory of irreversible processes. I. General theory and simple applications to magnetic and conduction problems, J. Phys. Soc. Jpn. **12**, 570 (1957).

[36] D. A. Greenwood, The Boltzmann equation in the theory of electrical conduction in metal, Proc. Phys. Soc., London **71**, 585 (1958).

[37] G. D. Mahan, *Many-Particle Physics, Physics of Solids and Liquids* (Springer, New York, 2000).

[38] J. Banhart, Optical Conductivity of Disordered Alloys Calculated from First Principles, Phys. Rev. Lett. **82**, 2139 (1999).

[39] I. Turek, J. Kudrnovský, V. Drchal, L. Szunyogh, and P. Weinberger, Interatomic electron transport by semiempirical and *ab initio* tight-binding approaches, Phys. Rev. B **65**, 125101 (2002).

[40] K. K. Saha and A. Mookerjee, Optical properties of random alloys: Application to CuAu and NiPt, J. Phys.: Condens. Matter **17**, 4559 (2005).

[41] H. Ebert, S. Mankovsky, K. Chadova, S. Polesya, J. Minár, and D. Ködderitzsch, Calculating linear-response functions for finite temperatures on the basis of the alloy analogy model, Phys. Rev. B **91**, 165132 (2015).

[42] W. H. Butler, Theory of electronic transport in random alloys: Korringa-Kohn-Rostoker coherent-potential approximation, Phys. Rev. B **31**, 3260 (1985).

[43] I. A. Abrikosov and H. L. Skriver, Self-consistent linear-muffin-tin-orbitals coherent-potential technique for bulk and surface calculations: Cu-Ni, Ag-Pd, and Au-Pt random alloys, Phys. Rev. B **47**, 16532 (1993).

[44] P. Hohenberg and W. Kohn, Inhomogeneous electron gas, Phys. Rev. **136**, B864 (1964).

[45] U. von Barth and L. Hedin, A local exchange-correlation potential for the spin polarized case, J. Phys. C: Solid State Phys. **5**, 1629 (1972).

[46] H. Ebert, S. Mankovsky, D. Ködderitzsch, and P. J. Kelly, *Ab initio* Calculation of the Gilbert Damping Parameter via the Linear Response Formalism, Phys. Rev. Lett. **107**, 066603 (2011).

[47] D. Ködderitzsch, K. Chadova, J. Minár, and H. Ebert, Impact of finite temperatures and correlations on the anomalous Hall conductivity from *ab initio* theory, New J. Phys. **15**, 053009 (2013).

[48] H. Terletska, Y. Zhang, K.-M. Tam, T. Berlijn, L. Chioncel, N. S. Vidhyadhiraja, and M. Jarrell, Systematic quantum cluster typical medium method for the study of localization in strongly disordered electronic systems, Appl. Sci. **8**, 2401 (2018).

[49] V. Dobrosavljevic, A. A. Pastor, and B. K. Nikolic, Typical medium theory of Anderson localization: A local order parameter approach to strong-disorder effects, Europhys. Lett. **62**, 76 (2003).

[50] B. C. Sales, K. Jin, H. Bei, G. M. Stocks, G. D. Samolyuk, A. F. May, and M. A. McGuire, Quantum critical behavior in a concentrated ternary solid solution, Sci. Rep. **6**, 26179 (2016).

[51] G. D. Samolyuk, L. K. Béland, G. M. Stocks, and R. E. Stoller, Electron–phonon coupling in Ni-based binary alloys with application to displacement cascade modeling, J. Phys.: Condens. Matter **28**, 175501 (2016).

[52] O. Gunnarsson, Stoner model in spin-density-functional formalism, Physica B+C (Amsterdam) **91**, 329 (1977).

[53] C. C. Homes, T. Timusk, X. Wu, Z. Altounian, A. Sahnoune, and J. O. Ström-Olsen, Optical Conductivity of the Stable Icosahedral Quasicrystal $Al_{63.5}Cu_{24.5}Fe_{12}$, Phys. Rev. Lett. **67**, 2694 (1991).

[54] Y. Cao, V. Fatemi, S. Fang, K. Watanabe, T. Taniguchi, E. Kaxiras, and P. Jarillo-Herrero, Unconventional superconductivity in magic-angle graphene superlattices, Nature **556**, 43 (2018).